

Supporting Information for

A General Hierarchical Flower-Shaped Cobalt
Oxide Spinel Template: Facile Method, Morphology
Control, and Enhanced Saturation Magnetization

Zheng Fu^{a,b}, Liang Qiao^a, Yang Liu^a, Zhengxi Xuan^{a,b}, Changning Li^a, Saranya Rajendra Pillai^a,

Chaeon Lee^a, Mark Swihart^{a,b}

^aDepartment of Chemical and Biological Engineering and ^bRENEW Institute, University at

Buffalo (SUNY), Buffalo, New York 14260, United States

Figure S1 provides a representative heating (temperature vs. time) curve used for most of the syntheses reported here. This gentle heating rate used in most cases is 2.7 °C/min, while the faster heating rate for sample Figure 1 A3 is 4.6 °C/min.

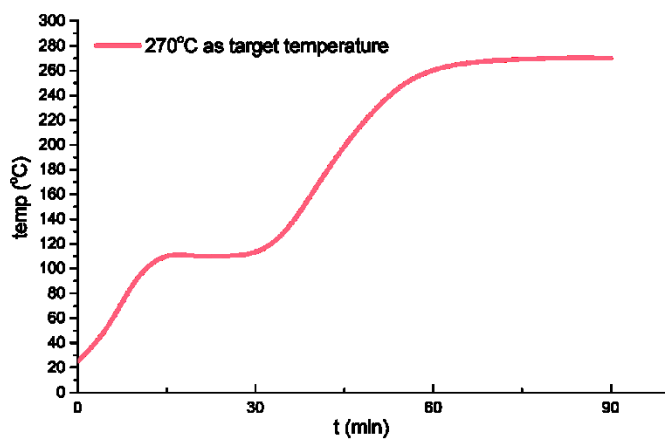


Figure S1. Representative heating curve for M-SCO synthesis.

Cobalt oxide nanocrystals show an irregular morphology (Figure S2) when synthesized without OA.

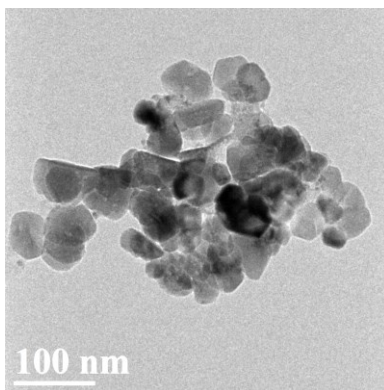


Figure S2. Irregular cobalt oxide nanoparticles synthesized without OA.

Figure S3 shows a typical lower-magnification TEM image of the SCO template to show the uniformity of size and structure of materials produced by this approach. The average size including arms of these NCs is around 195 nm. For flower-like structures the core crystallite size is around 52 nm, calculated from XRD peak broadening by the Scherrer equation¹, consistent with the TEM measurement. For cube star NCs like those shown in Figure 1 B2, B4, or B5, the average crystallite size calculated by the Scherrer equation was around 24 nm, reflecting the single cube star size observed in TEM images.

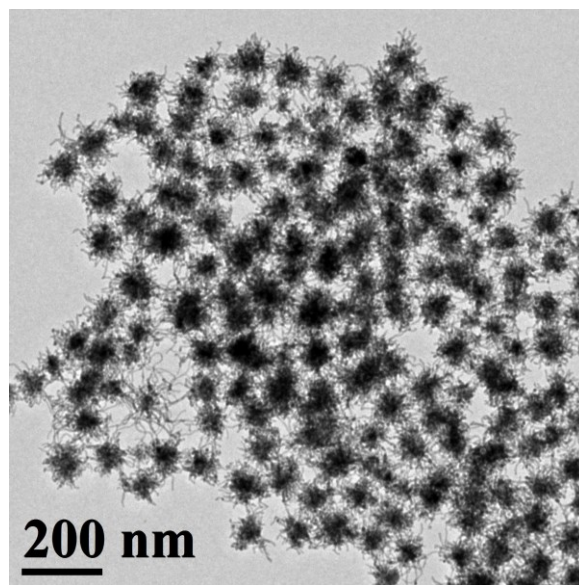


Figure S3. A zoom-out TEM image of SCO template.

While all M-SCO samples presented in the main manuscript were synthesized in one step, we also applied normal two-step templating methods to synthesize Fe-SCO and Ni-SCO. First, the SCO template was synthesized with the same recipe as for sample Figure 1 A11 without any Fe or Ni precursors. Next, Fe or Ni precursors are mixed with the SCO template and the same ligands and additives as Fe-SCO and Ni-SCO. As shown as Figure S4, the SCO template maintained the original flower-like morphology. However, XRD patterns show that these two samples are both of $\text{Co}_3\text{O}_4/\text{Fe}_2\text{O}_3$ and $\text{Co}_3\text{O}_4/\text{NiO}$, respectively. Both TEM and XRD results demonstrate that the more common two-step templating method is not suitable to synthesize M-SCO. This result also illustrates the stability and extensibility of the SCO template, based on which the mixture of $\text{Fe}_2\text{O}_3@\text{SCO}$ template and $\text{NiO}@\text{SCO}$ template are synthesized with original flower-like morphology.

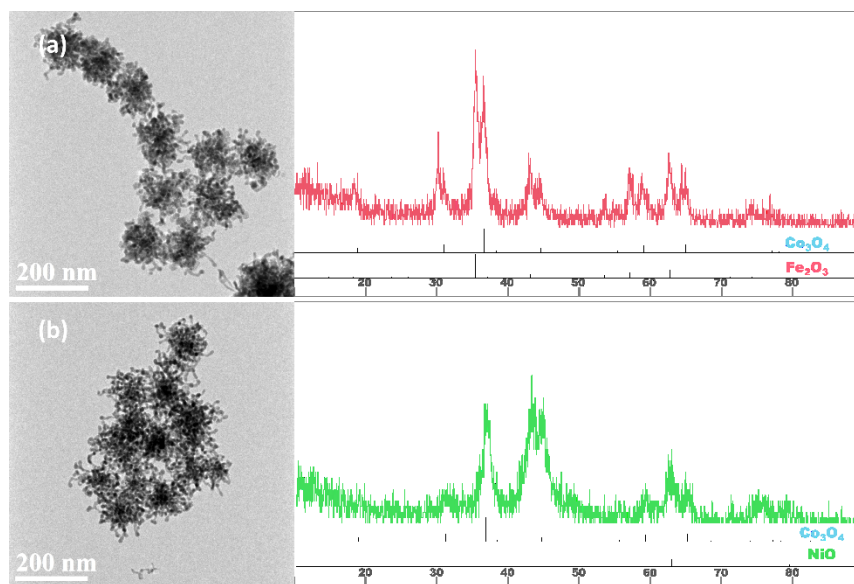


Figure S4. TEM images and XRD patterns of (a) $\text{Co}_3\text{O}_4/\text{Fe}_2\text{O}_3$ and (b) $\text{Co}_3\text{O}_4/\text{NiO}$ synthesized in two steps: (1) normal SCO template synthesis, as in Figure 1 A11; followed by (2) Fe or Ni precursor addition to the SCO template under the same conditions.

The density of sample FNC(a) and FNC(b) at room temperature and after annealing in argon at 300°C heating were tested, yielding the results shown in Table S1. The specific surface area of a mixture of samples including SCO, Fe-SCO, and Ni-SCO is shown in Table S2.

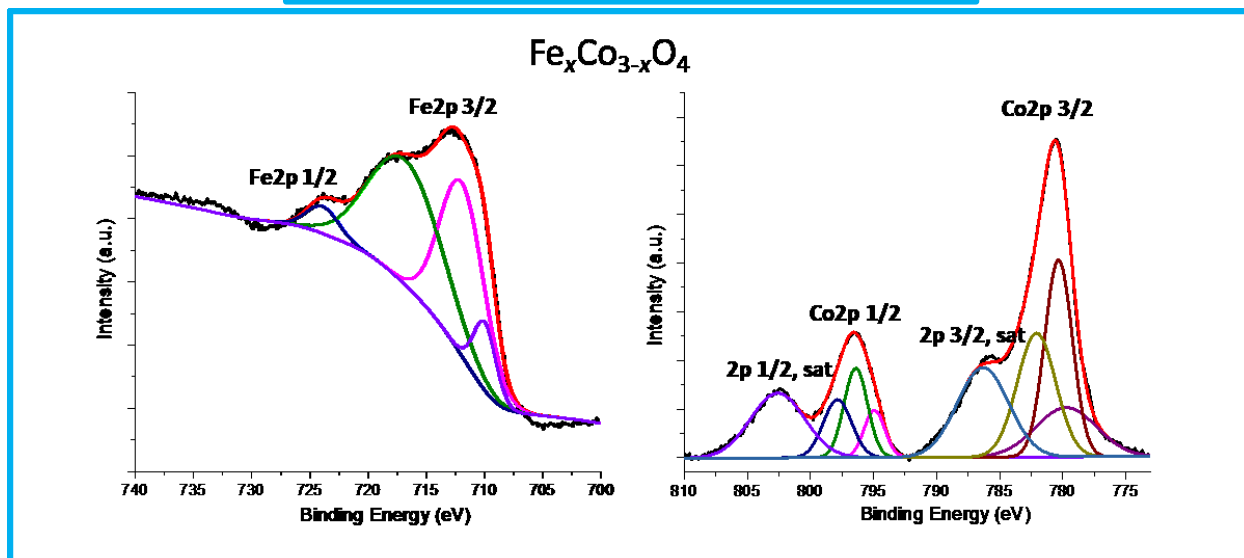
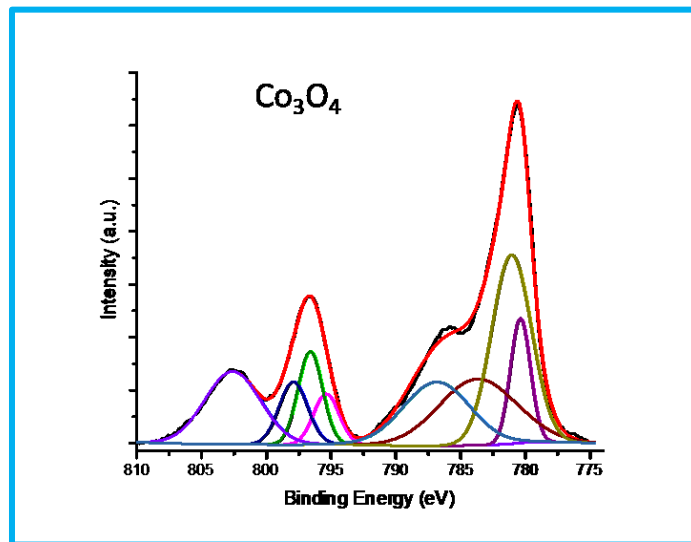
Table S1. Densities measured by helium pycnometry for samples FNC (a) and (b) before and after the 300°C annealing treatment, as shown in Figure 5.

	FNC (a)	FNC (b)
Density at room temperature (g/cm ³)	3.67	3.91
Density after 300°C annealing (g/cm ³)	5.47	5.22

Table S2. Specific surface area (SSA) of mixed products M-SCO at both room temperature and 300°C annealing treatment.

	M-SCO at room temperature	M-SCO after 300°C annealing
Specific surface area (m ² /g)	50.912	36.134

X-ray photoelectron spectroscopy (XPS) measurements were made for five main samples as shown in Figure S5.



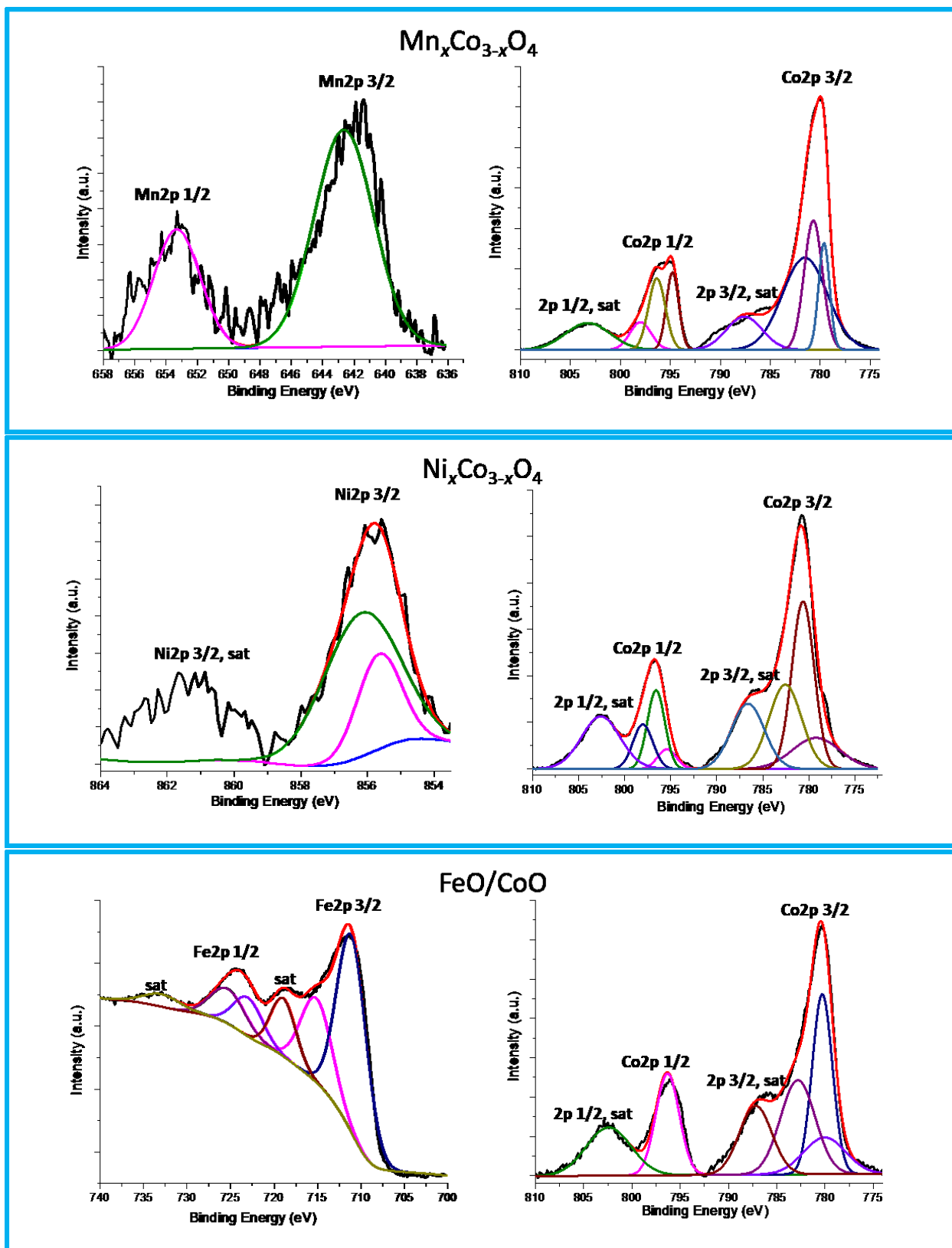


Figure S5. XPS spectra for M-SCO samples shown on Figure 2.

Table S3. Analysis of M:Co (M= Fe, Mn, Ni) atomic ratios measured by EDS and XPS for FeCo₂O₄, MnCo₂O₄, NiCo₂O₄, and FeO/CoO samples.

Ref.	Figure2. (b)	Figure2. (c)	Figure2. (d)	Figure2. (e)
Material composition	FeCo ₂ O ₄	MnCo ₂ O ₄	NiCo ₂ O ₄	FeO/CoO
Elemental ratio	Fe: Co	Mn: Co	Ni: Co	Fe: Co
EDS atomic ratio	0.15	0.02	0.2	0.81
XPS atomic ratio	0.025	0.016	0.022	0.17

Table S4. Comparison of the composition, saturation magnetization, and synthesis method of cobalt spinel oxides reported in recent years.²⁻¹¹

#	Composition	Saturation magnetization (emu/g)	Synthesis method	Reference
1	CoFe ₂ O ₄	65 - 80	Seed-mediated growth	2
2	CoFe ₂ O ₄	80	Complexometric synthesis	3
3	CoFe ₂ O ₄	72.95	Reverse coprecipitation	4
4	Ni _{0.4} Co _{0.6} Er _x Fe _{2-x} O ₄	35.99 - 39.95	Surfactant-assisted co-precipitation route	5
5	Co _{1-x} Ni _x Fe ₂ O ₄	47.6 - 84.5	Aerosol route	6
6	Co _x Zn _{1-x} Fe ₂ O ₄	50.0 - 92.3	Electrospinning method	7
7	Co _{1-x} Ni _x Fe ₂ O ₄	41.75 - 76.08	Solution combustion route	8
8	Ni _{0.4} Zn _{0.6} Co _{0.1} Fe _{1.9} O ₄	32 - 57	Co-precipitation method	9
9	Mn _x Co _{3-x} O ₄	< 1	Air plasma spray process	10
10	Ni _{1-x} Co _x Mn _y Fe _{2-y} O ₄	21.81 - 48.89	Sol-gel combustion method	11

Systematic study of M-SCO nanostructures

The stability and extensibility of this SCO template is outstanding. Representative TEM images of all of the M-SCOs that we have synthesized to date are shown in Figure 6. Including five M-SCOs that we discussed above in greater detail, 23 types of M-SCOs with hierarchical flower shapes are synthesized via one-step method from readily available precursors. We are confident that even more types of M-SCOs with this flowerlike structure can be produced following the common guidance of M-SCO synthesis provided here. The synthesis all these M-SCOs one can use different ratios of Co:M to control the stability of the 3D flower morphology. As we discussed in the morphology atlas part, the doped M element has varied effects on the SCO template. For example, the usual Fe-SCO with flower shape like sample B8 was obtained with a precursor ratio of Co:Fe=1:0.5 to achieve the AB_2O_4 spinel structure. However, the stability of the SCO template may vary for different doping metal elements. Sample D4 with the precursor ratio of Co:Ni=1:0.3 led to small spheres, rather than a flower-like morphology, due to the higher Ni content. Therefore, we tuned the precursor ratio to maintain the SCO template with 3D flower morphology while incorporating various metals for their own properties.

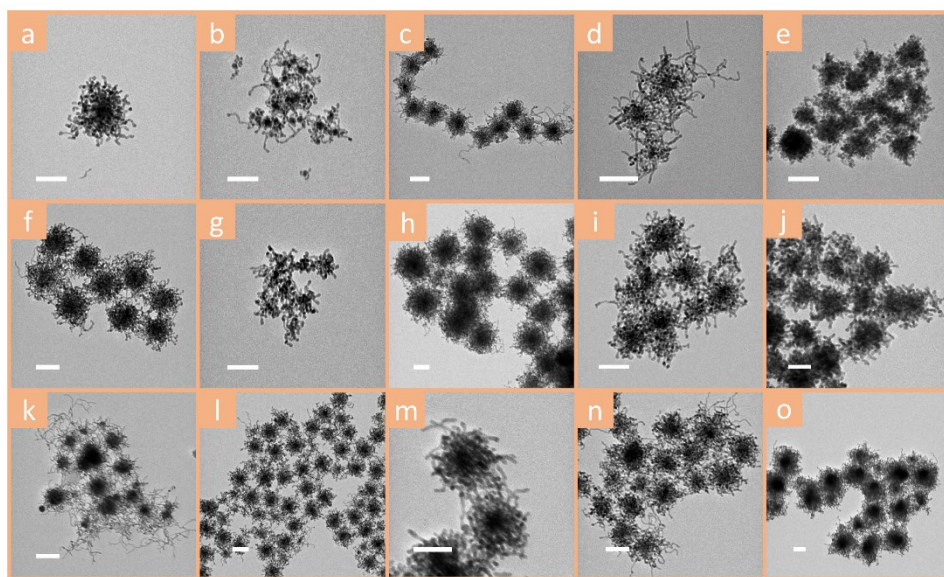
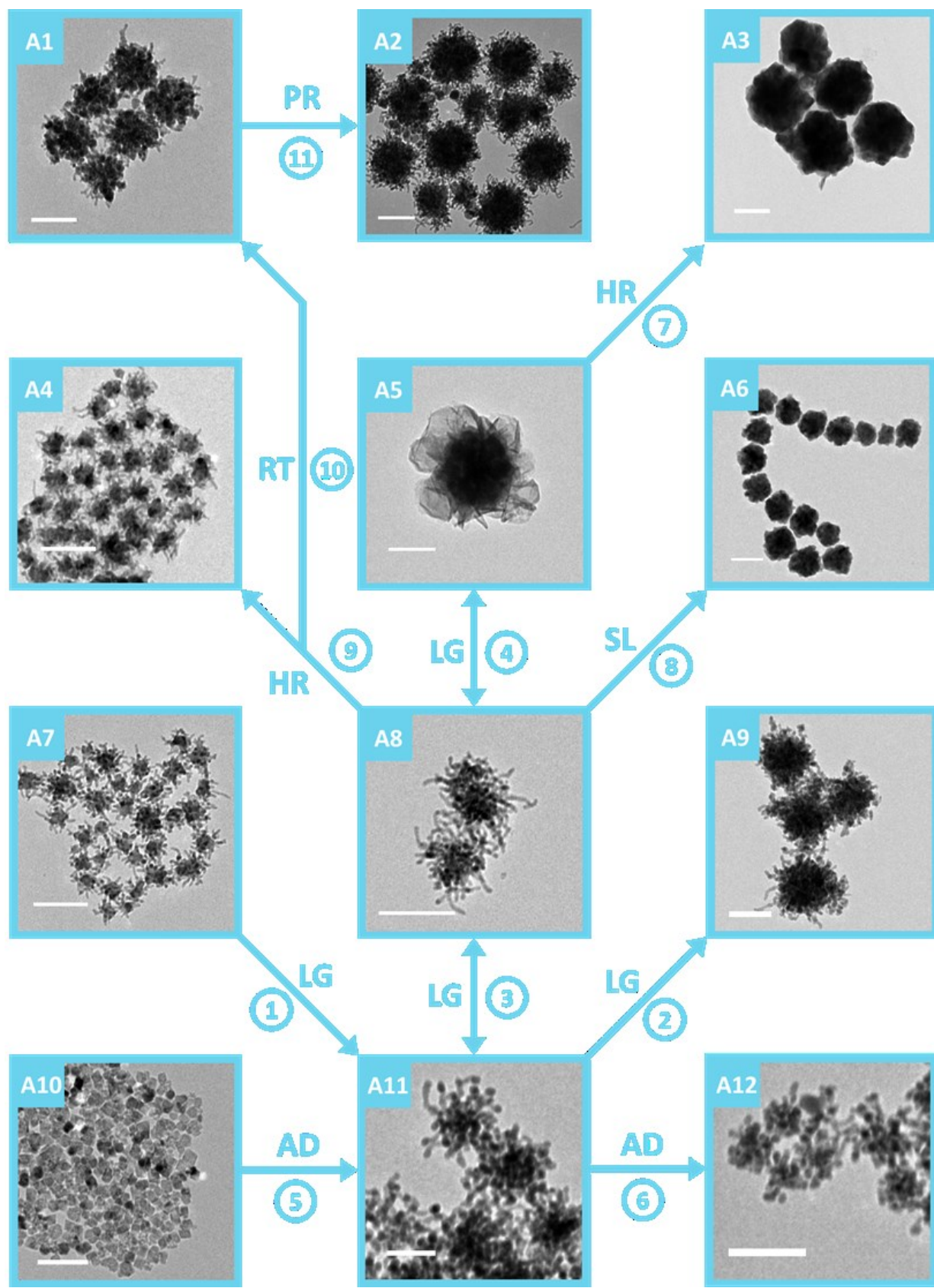


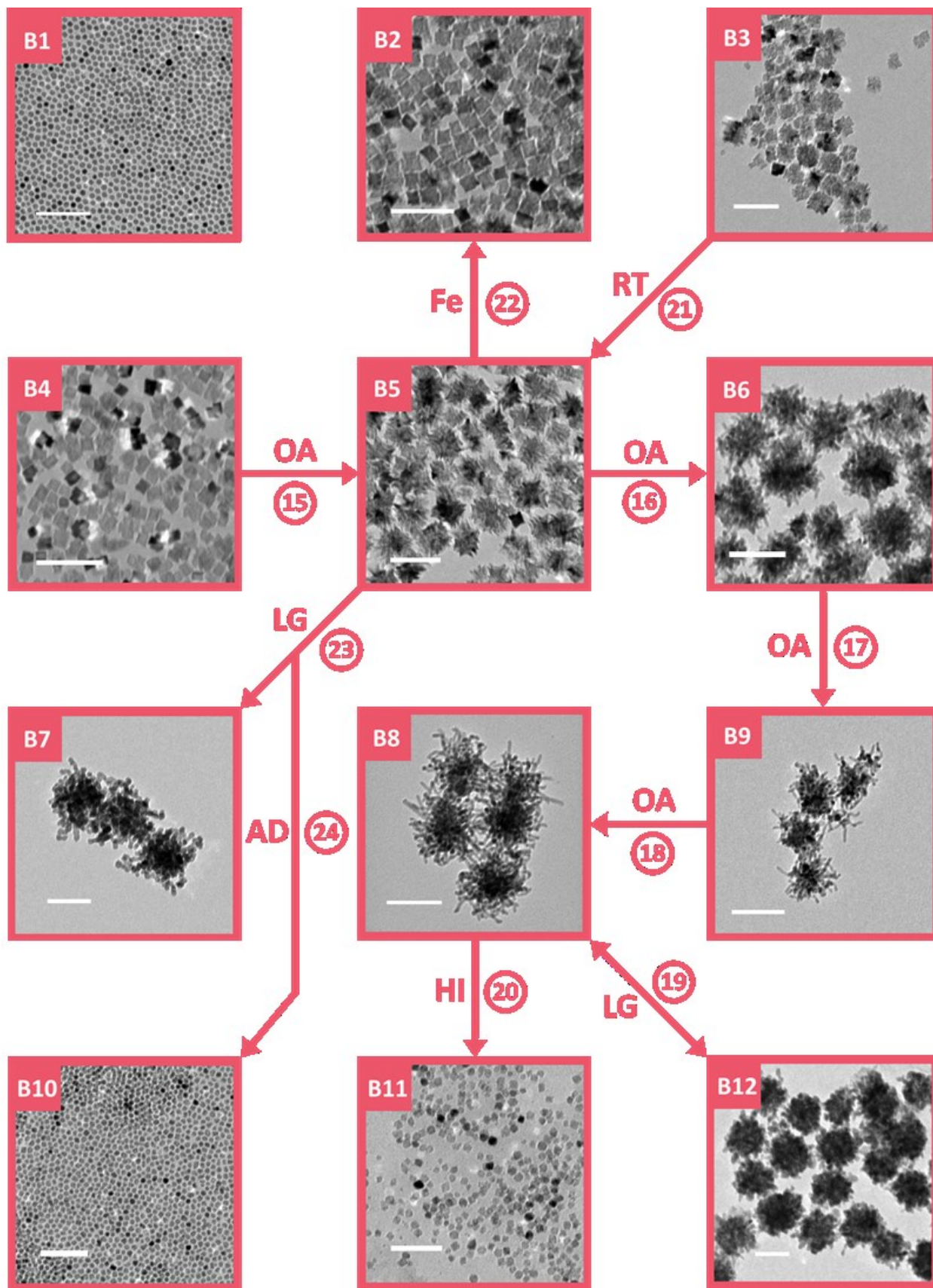
Fig. S6 TEM images of a) Cu-SCO, b) Ag-SCO, c) Ti-SCO, d) Li-SCO, e) K-SCO, f) Zn-SCO, g) Pd-SCO, h) Mo-SCO, i) Gd-SCO, j) Pt-SCO, k) Ga-SCO, l) Al-SCO, m) Cr-SCO, n) Fe-SCO, o) Ag-Cu-SCO. The detailed synthesis strategy is listed in the excel file. Scale bars are 100 nm.

Although all these M-SCOs show hierarchical flower shapes, their stability, detailed shapes, and sizes are affected by the doping metals, which are incorporated to different extents for different metals. For example, b) Ag-SCO and g) Pd-SCO produce nanoflowers that are generally smaller than for other compositions. On the contrary, upon introduction of Ti, Mo, and Ag/Cu to produce c) Ti-SCO, h) Mo-SCO and o) Ag-Cu-SCO, the flower size is enlarged by a factor of 2 to 3. Among the tested dopants, only potassium was not incorporated into the flower-like structure. EDS measurements did not detect any K in the K-SCO sample, indicating that any potassium present is at a level below the detection limit of EDS. The final flower shaped SCO is still produced with the addition of K precursor, reflecting the robustness of the SCO template. We also tried different precursors such as ferrocene as iron source to synthesize Fe-SCO

(Figure 6 n). Li-SCO presented here suggests a new approach to make lithium cobalt oxide (LCO)-based cathode materials for lithium ion batteries, using SCO template to obtain flower shape LCO.

These diverse M-SCO materials can combine at least two properties of the dopant atom (M) property and SCO magnetic property. For example, the noble metal-doped M-SCOs might perform well in electrocatalysis, and Cu-SCO may have good thermal and electrical conductivity, and so on. Thus, we expected this promising magnetic SCO template can be more deeply explored for a broad range of applications in the near future.





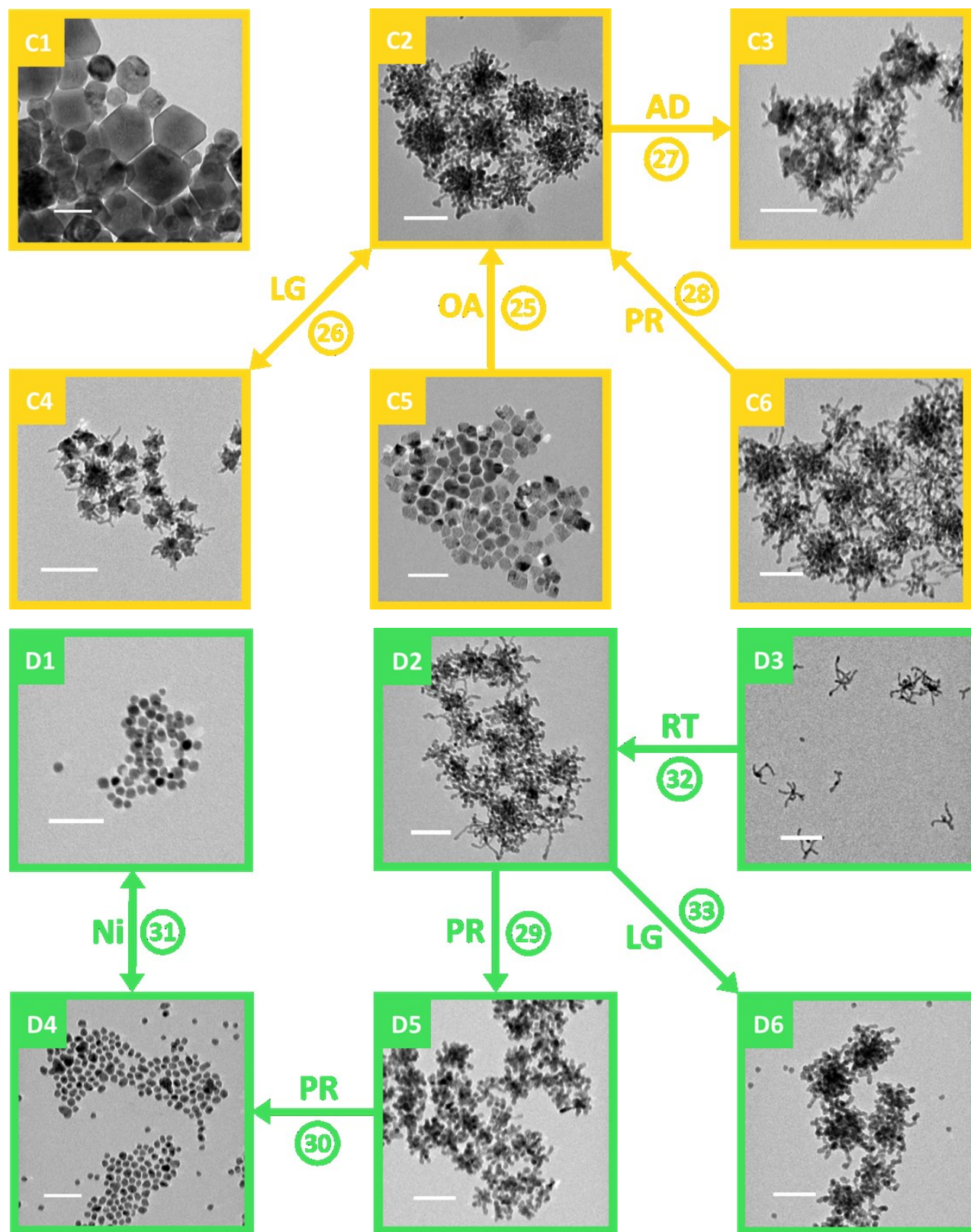


Fig. S7. Enlarged view, in four parts, of the TEM atlas of Fig. 1 of the main manuscript.

References

1. P. Scherrer, in *Kolloidchemie Ein Lehrbuch*, Springer, 1912, 387.
2. Q. Song and Z. J. Zhang, *Journal of the American Chemical Society*, 2004, **126**, 6164.
3. P. D. Thang, G. Rijnders and D. H. Blank, *J. Magn. Magn. Mater.*, 2005, **295**, 251.
4. F. Huixia, C. Baiyi, Z. Deyi, Z. Jianqiang and T. Lin, *J. Magn. Magn. Mater.*, 2014, **356**, 68.
5. M. F. Warsi, A. Iftikhar, M. A. Yousuf, M. I. Sarwar, S. Yousaf, S. Haider, M. F. Aly Aboud, I. Shakir and S. Zulfiqar, *Ceram. Int.*, 2020, **46**, 24194.
6. S. Singhal, J. Singh, S. K. Barthwal and K. Chandra, *J. Solid State Chem.*, 2005, **178**, 3183.
7. X. Huang, J. Zhang, S. Xiao and G. Chen, *J. Am. Ceram. Soc.*, 2014, **97**, 1363.
8. K. M. Srinivasamurthy, J. Angadi V, S. P. Kubrin, S. Matteppanavar, D. A. Sarychev, P. M. Kumar, H. W. Azale and B. Rudraswamy, *Ceram. Int.*, 2018, **44**, 9194.
9. A. Thakur, P. Thakur and J.-H. Hsu, *J. Appl. Phys.*, 2012, **111**, 07A305.
10. S. J. Han, Z. Pala and S. Sampath, *J. Power Sources*, 2016, **304**, 234.
11. H. Arabi and F. Ganjali, *J. Supercond. Novel Magn.*, 2013, **26**, 1031.